Journal of Catalysis **208,** 238–246 (2002)
doi:10.1006/jcat.2002.3562, available online at http://www.idealibrary.com on IDEAL®

Vanadium Phosphorus Oxide Catalyst Modified by Niobium Doping for Mild Oxidation of *n*-Butane to Maleic Anhydride

Andréa M. Duarte de Farias,*,† Wilma de A. Gonzalez,* Paulo G. Pries de Oliveira,† Jean-Guillaume Eon,‡ Jean-Marie Herrmann,§ Mimoun Aouine,¶ Stéphane Loridant,¶ and Jean-Claude Volta¶,[1]

*Instituto Militar de Engenharia, Pça Gen. Tiburcio, 80, Rio de Janeiro, RJ, Brazil; †Instituto Nacional de Tecnologia, Laboratorio de Catalise, Av. Venezuela, 82, Rio de Janeiro, RJ, Brazil; ‡Universidade Federal do Rio de Janeiro, Inst de Quimica, Bl. A, Cidade Universitaria, Rio de Janeiro, RJ, Brazil; §Ecole Centrale de Lyon, Laboratoire de Photocatalyse, Catalyse et Environnement, IFOS, CNRS, BP 163, 69131, Ecully Cedex, France; and ¶Institut de Recherches sur la Catalyse, 2 Avenue Albert Einstein, 69626, Villeurbanne Cédex, France

Received December 3, 2001; revised February 14, 2002; accepted February 14, 2002

The interest of doping $(VO)_2P_2O_7$ with Nb^{5+} ions has been studied for *n*-butane oxidation to maleic anhydride. Nb was solubilized as niobium (V) ethoxide into isobutanol and used as a reducing reagent to prepare the $VOHPO_4 \cdot 0.5H_2O$ precursor. Under *n*-butane fuel-lean oxidation conditions, the VNbPO precursor was activated at a temperature 20°C lower than for undoped VPO because of a modification of its morphology. Electron microscopy showed that the activated VNbPO catalyst is more disorganized than the activated VPO. It contains more defects and concentrates Nb at the surface. Nb acts as an *n*-type dopant for the *p*-type $(VO)_2P_2O_7$ semiconductor, as observed in electrical conductivity measurements. ^{31}P NMR by spin-echo mapping and XPS spectroscopy provide evidence that the VNbPO catalyst is more oxidized, particularly at the surface. Doping with Nb creates defects, responsible for C–H *n*-butane activation, which have been observed to be associated with Lewis acid sites of low acidity. This is the reason for the enhancement of the *n*-butane conversion. Selectivity to maleic anhydride is not modified by Nb-doping while CO_2/CO formation is increased due to the higher surface V^{5+}/V^{4+} ratio.

***Key Words:* *n*-butane mild oxidation; maleic anhydride; vanadium phosphorus oxide; niobium doping.**

INTRODUCTION

Vanadium phosphorus oxide catalysts (VPO) are known to catalyze the mild oxidation of *n*-butane to maleic anhydride (MA) (1–3). Catalytic performance may be improved by adding specific doping agents to the VPO composition, but their effect on conversion and selectivity may be different. The nature, the location, and the role of these dopants have been previously reviewed in the open literature (4). For example, it was observed that the presence of Co changes the surface properties by modifying the redox properties of the VPO catalyst, which results in an easier desorption of maleic anhydride and a higher selectivity to mild oxidation (5). The effect of Fe doping has been compared to that of Co in fuel-lean oxidation of *n*-butane (6, 7): both dopants improve the selectivity to MA, but Co decreases *n*-butane conversion whereas Fe increases it. These results were explained by a different dispersion of the $VOPO_4/(VO)_2P_2O_7$ phases during the period of activation of the precursor. By electron microscopy and ^{31}P NMR by spin-echo mapping, it was observed that Co delays the transformation of the precursor, increasing the disorder of the VPO material at lower temperature by stabilizing an amorphous VPO phase for which Co was acting as the promoter (8). Co was also observed to be an efficient dopant for the VPO catalyst in fuel-rich *n*-butane oxidation conditions, making possible the mild oxidation of *n*-butane to MA; this was observed to be impossible without this dopant (9).

Many other dopants of VPO have been considered to improve the catalytic performance in fuel-lean oxidation conditions (4). There is not a general explanation concerning their specific role and the examination of the published results shows that they should affect differently the nature and the distribution of the nanocrystalline oxidized $VOPO_4$ phases which are generated during the activation period of the catalyst and affect the properties of the equilibrated catalyst (10, 11). Among these dopants, Nb has not yet been seriously considered, although it is mentioned in a patent assigned to ICI for mild oxidation of *n*-butane to MA (12). Apart from this, a promotional catalytic effect of niobium phosphate for vanadyl pyrophosphate was observed for mild oxidation of *n*-butane: the authors explained this result by considering the development of strong Lewis acid sites induced by Nb and associated to the formation of a $(V_{1-x}Nb_xO)_2(P_2O_7)_{1-x}(PO_4)_{2x}$ solid solution (13). We showed that this interaction in close proximity to V should occur for the $VOHPO_4 \cdot 0.5H_2O$ precursor, which was modified by amorphous niobium phosphate: a new signal was detected by ^{31}P NMR (MAS and spin-echo mapping) on the corresponding VPO precursor (14).

[1] To whom correspondence should be addressed.

0021-9517/02 $35.00

In the present publication, the transformations induced by Nb doping of the VPO precursor have been investigated, as well as the effect on the catalytic properties and on the physicochemical characteristics of the corresponding catalyst for *n*-butane oxidation to maleic anhydride. This work is in the continuation study demonstrating the interest of associating Nb with V in mixed oxides catalysts for mild oxidation of light hydrocarbons (15, 16).

EXPERIMENTAL

A reference $VOHPO_4 \cdot 0.5H_2O$ precursor (designated VPO) was prepared according to the organic route by refluxing a suspension of V_2O_5 (11.5 g) into isobutanol (250 ml) in the presence of 85% H_3PO_4 with a P/V ratio = 1 : 1 for 16 h (17). A VPO precursor modified by niobium (designated VNbPO) was prepared according to the same procedure by solubilizing niobium(V) ethoxide into isobutanol (Nb/V = 0.01). All the operations of refluxing were similar to those used for reference $VOHPO_4 \cdot 0.5H_2O$ precursor. The two resulting blue solids were recovered by filtration, washed with fresh isobutanol and ethanol, and finally dried in air for 16 h at 110°C. Chemical analysis was performed by atomic emission spectroscopy with an ICP spectro-flame (inducting coupling plasma) from SPECTRO after dissolution of the solids in hydrochloric acid.

The BET specific surface areas of the solids were conventionally measured by N_2 adsorption at 77.4 K. The decomposition of the two precursors under air was followed in a SETARAM TGA–DTA 92 thermobalance from room temperature up to 700°C at a heating rate of 5°C/min.

Activation under reaction conditions over 80 h was conducted in order to obtain activated solids which were then studied by XRD, SEM, TEM, NMR, Raman spectroscopy, electrical conductivity, and acidity measurements. X-ray diffraction (XRD) patterns were collected with a SIEMENS D500 diffractometer using Cu $K\alpha$ radiation. For transmission electron microscopy (TEM), the catalysts were sonically dispersed in ethanol and deposited on a copper grid coated with holey carbon before examination in a JEOL 2010 microscope with a high-resolution pole piece. Microanalyses were performed with a link Isis system. A HITACHI S 800 microscope was used for SEM examination of the VPO precursors. Samples for SEM examination were deposited on a metallic grid and then sputtered with gold. The ^{31}P NMR spectra were recorded with a BRUCKER DSX400 spectrometer, at 161.9 MHz, equipped with a standard 4-mm probe head. The ^{31}P spin-echo mapping (SEM) spectra were obtained with a sweep width of 2 mHz, t = 20 ms, and 90° pulse length of 1.5 ms. Raman spectra were recorded with a DILOR XY spectrometer. The excitation line at 514.53 nm of an argon–krypton laser was used with a power of 0.5–1 mW on the sample. It has been checked that such a power is low enough to avoid heating effects by the laser beam. XPS examinations of the VPO catalysts were performed with an ESCALAB 200R spectrometer using Al $K\alpha$ radiation. The binding energy of adventitious carbon was taken as a reference at 284.5 eV. Examinations were focused on the binding energies of P 2p, C 1s, V $2p_{3/2}$ (V^{5+} and V^{4+}), Nb 3d, and O 1s. Electrical conductivity measurements were performed in a previously decribed cell (18), especially designed to study electronic interactions between powdered samples under various atmospheres. VPO catalysts were heated in air up to 400°C at a heating rate of 5°C/min. Conductivity measurements were then followed at 400°C as a function of time. Acidity measurements on VPO catalysts were performed by thermodesorption of pyridine, used as a basic probe. Catalysts were compressed to obtain disks of 25 mg. After outgassing at 350°C, pyridine was adsorbed at room temperature. The catalysts were further outgassed at 25, 100, 150, 200, 250, 300, and 350°C. The acid properties were then compared by measurement of the intensity of the characteristic bands at 1540 cm^{-1} (Brønsted acid site) and at 1450 cm^{-1} (Lewis acid site) as a function of the temperature of outgassing.

Catalytic tests were conducted on 1 ml of precursor at 400°C and atmospheric pressure in a differential flow Pyrex microreactor. The VPO and VNbPO precursors were activated on line for 80 h under fuel-lean oxidation conditions (n-$C_4H_{10}/O_2/He$ = 1.6/18.0/80.4) at 2000 h^{-1} GHSV from 25°C up to 400°C at a heating rate of 0.5°C/min. Catalytic performances (*n*-butane conversion and MA, CO, CO_2 selectivities) were compared at 400°C as a function of time of testing of the VPO and VNbPO catalysts. Reactants and reaction products were analyzed online by gas chromatography. O_2, CO, CO_2, H_2O, and He were detected by thermal catharometry after separation on a 4 m × 1/8 in. 80- to 100-mesh Carbosieve B column. Hydrocarbons were detected by flame ionization after separation on a 4 m × 1/8 in. 80- to 100-mesh Durapak column. Maleic anhydride, aldehydes, and acids were detected by flame ionization after separation on a 2 m × 1/8 in. 80- to 100-mesh, 10% AT 1200-imp. 1% H_3PO_4/Chromosorb WAW column.

RESULTS AND DISCUSSION

The BET areas of the VNbPO and VPO precursors were both observed to be 7 m^2/g. Activated catalysts showed surface areas of 17 and 12 m^2/g for VNbPO and VPO, respectively. Figure 1 shows the XRD patterns of the VPO and VNbPO precursors. Both are characteristic of the $VOHPO_4 \cdot 0.5H_2O$ precursor phase only (17). The modification of the relative intensity of the (001) and (220) lines for the VNbPO precursor as compared to the VPO precursor is indicative of a difference of morphology of the $VOHPO_4 \cdot 0.5H_2O$ platelets induced by the presence of Nb, which was confirmed by SEM examination (Fig. 2). In the

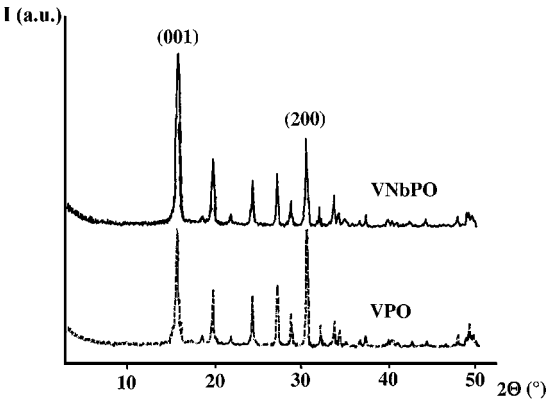

FIG. 1. XRD patterns of the VNbPO and VPO precursors.

case of VNbPO, the platelets of the precursor are smaller and do not agglomerate into sand roses, as seen for VPO. Chemical analysis confirmed the presence of Nb with the expected composition (Nb/V = 0.0102). Nb is well dispersed throughout the bulk of $VOHPO_4 \cdot 0.5H_2O$, as observed by EDX in a TEM.

It is known (19) that the decomposition under air of $VOHPO_4 \cdot 0.5H_2O$ to $(VO)_2P_2O_7$ occurs in two steps. The vanadium hemihydrate retains its water of hydration up to 360°C. The departure of this water molecule results in vacancy formation at the apex of the vanadium–oxygen octahedra. At this stage, an electronic rearrangement proceeds, which corresponds to the formation of $VOHPO_4$ layers (Eq. [1]). These layers subsequently join, expelling the constitutional water molecules to form one P_2O_7 group from two HPO_4 groups (Eq. [2]). $(VO)_2P_2O_7$ is then further oxidized to $VOPO_4$ (step [3]). All these transformation steps were identified by XRD examination of the samples (19). The process of dehydration–oxidation under air may be summarized by the corresponding scheme:

$$VOHPO_4 \cdot 0.5H_2O \rightarrow VOHPO_4 + 0.5H_2O, \quad [1]$$

$$2VOHPO_4 \rightarrow (VO)_2P_2O_7 + H_2O, \quad [2]$$

$$(VO)_2P_2O_7 + 1/2O_2 \rightarrow 2VOPO_4. \quad [3]$$

The decomposition under air of the VNbPO precursor is compared to that of VPO in Fig. 3. While the departure of water of hydration (endothermic process) occurs at the same temperature (360°C), the second departure of constitutional water molecules from the VNbPO precursor under air is lower by 21°C (414°C for VNbPO as compared to 435°C for VPO). Differences are also observed for the exothermic oxidation stage to $VOPO_4$(510°C for VNbPO as compared to 555°C for VPO). This is another indication of the differences between the VNbPO and VPO morphologies. Note that in the case of Co doping of VPO, a contrary result was observed with the dehydration step delayed instead of accelerated (19).

Figure 4 shows the variation of the *n*-butane conversion of the two catalysts with time when activated under the *n*-C_4/O_2/He flow. While conversion is similar in the first 20 h, the VNbPO catalyst shows significantly higher conversion in the next 60 h as compared to the VPO catalyst. After 80 h of activation, the *n*-C_4 conversion is 75% for VNbPO as compared to only 58% for VPO. Maleic anhydride was observed to be the only mild oxidation product for both VNbPO and VPO. Almost no acetic nor acrylic acids (less than 1%) were observed in both cases. Only CO and CO_2 were detected as total oxidation products. Figure 5 shows that almost no modification of the MA selectivity is observed between the two catalysts. However, Table 1 shows that the ratio CO_2/CO is higher for the VNbPO catalyst as compared to the VPO one.

Figure 6 shows the XRD pattern of the two catalysts after being activated. Both are very similar and are characteristic of a disorganized $(VO)_2P_2O_7$ phase with the (200), (024), and (032) lines at 23.00, 28.45, and 29.95°, respectively. In the case of VNbPO, the (200) reflection is broadened as compared to the (200) line for VPO. This result may be interpreted as due to a decrease in the size of the $(VO)_2P_2O_7$ crystallites in the [100] direction, in accordance with the modification of the $(VO)_2P_2O_7$ crystal morphology observed by SEM. Another possibility is peak overlap due to the presence of some residual $VOPO_4$ phases: on reference phases (20), the intense (111) and (012) lines of δ-$VOPO_4$ are observed at 22.08 and 24.17°, whereas the intense (004), (221), and (040) lines of γ-$VOPO_4$ are observed at 21.37, 22.66, and 23.16°, respectively (20). Moreover, the background in the XRD pattern of VNbPO appears to be slightly higher than in the case of VPO.

Figure 7 shows the Raman spectra of the two catalysts. For both samples, the background is probably due to electronic defects. Its curved aspect may correspond to the presence of an amorphous phase. Bands observed at 924, 1125, and 1181 cm^{-1} are typical of the $(VO)_2P_2O_7$ phase (20). The lower relative intensity of the 924-cm^{-1} band from VNbPO is linked to a lower crystallinity (21). In the case of VPO, the higher crystallinity may be due to a polarization effect appearing with the particular growth of crystallites. The spectrum of VNbPO does not show evidence for bands due to $NbOPO_4$ although the Raman response of this phase is much higher than $(VO)_2P_2O_7$. Indeed, we detected the presence of niobium phosphate by micro-Raman

TABLE 1

Catalytic Performance of VNbPO and VPO Catalysts Measured at 400°C after 80 h Activation under *n*-C_4/O_2/He = 1.6/18.0/80.4 at GHSV 2000 h^{-1}

Catalyst	Conv C_4 (%)	S_{MA} (%)	S_{CO} (%)	S_{CO_2} (%)
VNbPO	75.0	70.1	18.9	11.0
VPO	58.0	70.0	20.6	9.4

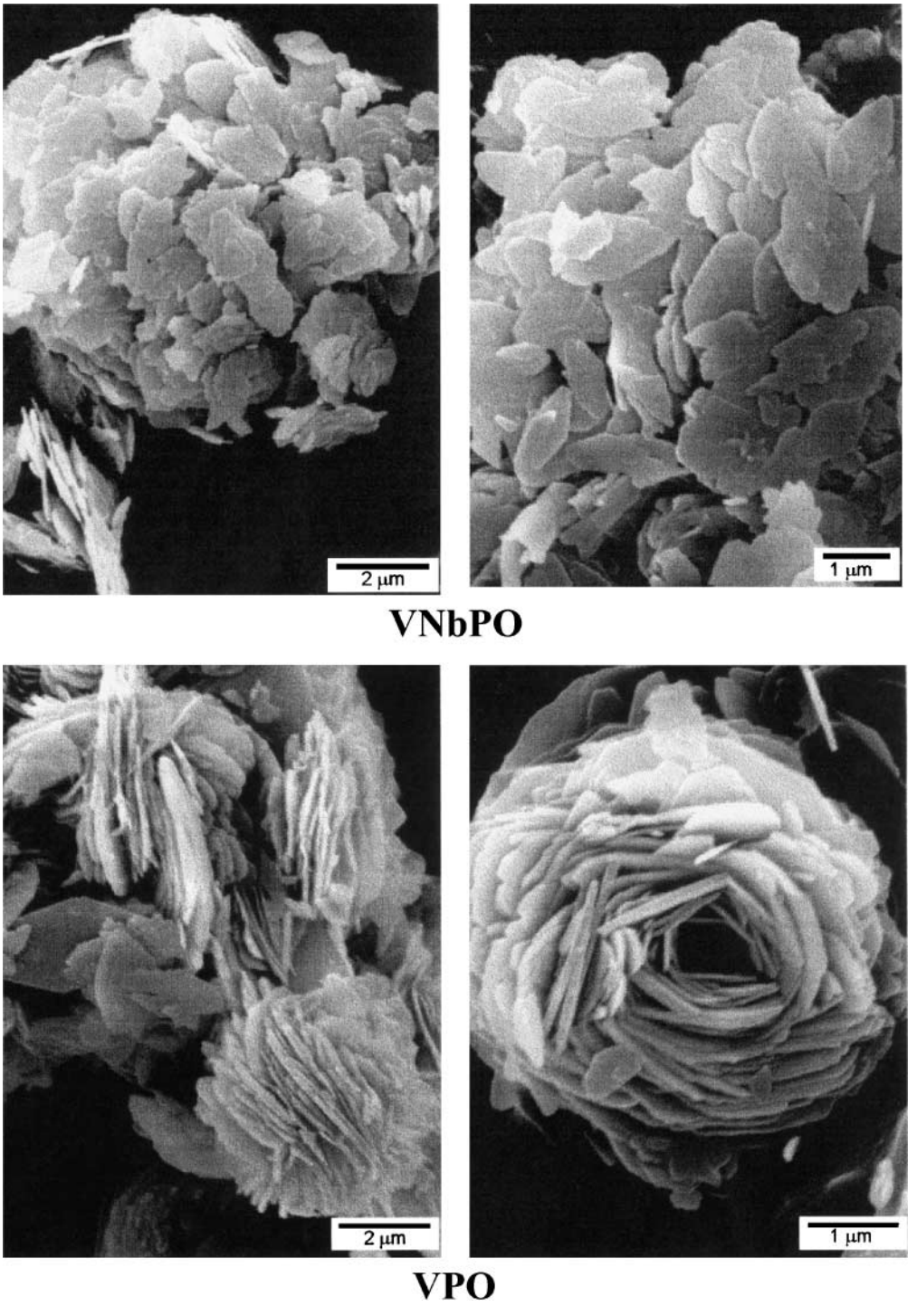

FIG. 2. Scanning electron micrographs of VNbPO and VPO precursors.

spectroscopy on samples synthesized by a different route, even at levels as low as 0.25% Nb/V. Finally, bands observed at about 1040 and 1075 cm^{-1} may be indicative of the presence of some $VOPO_4$ phases (20).

^{31}P NMR by spin-echo mapping gives information about the different oxidation states of vanadium surrounding the P atoms in $(VO)_2P_2O_7$ (22). Indeed V^{4+} in the $(VO)_2P_2O_7$ structure gives rise to a large signal around 2400–2700 ppm, depending on temperature of calcination. When cooling $(VO)_2P_2O_7$ at −123°C, this large signal has been observed to be split into four distinct signals, at 3200, 3650, 4200, and 4850 ppm. These signals have been attributed to the

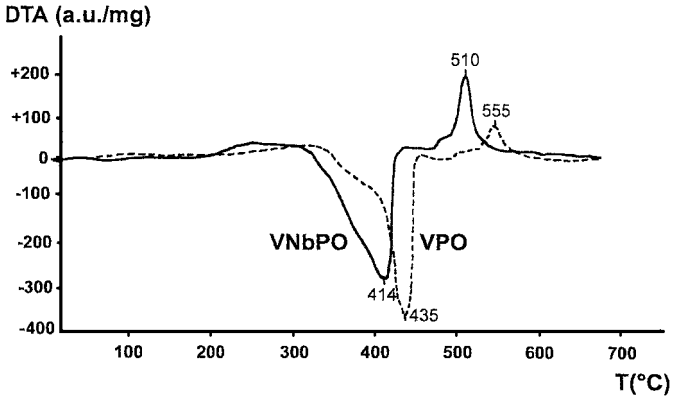

FIG. 3. DTA profiles of the decomposition of the VNbPO and VPO precursors under air.

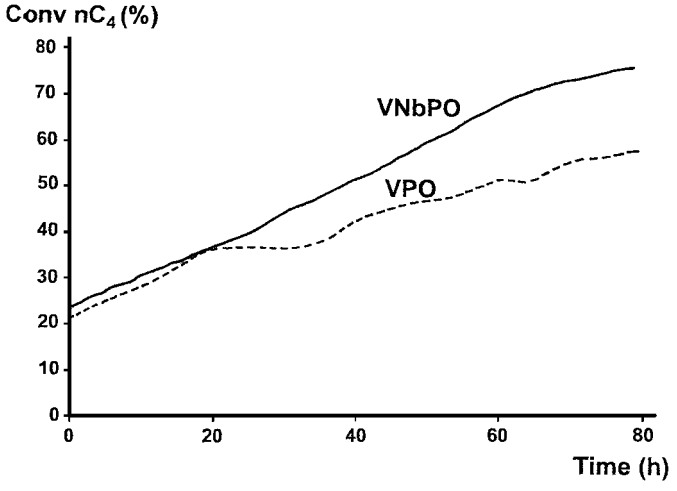

FIG. 4. Conversion of *n*-butane measured at 400°C under *n*-$C_4/O_2/He = 1.6/18.0/80.4$ at GHSV 2000 h^{-1} for the VNbPO and VPO catalysts as a function of time.

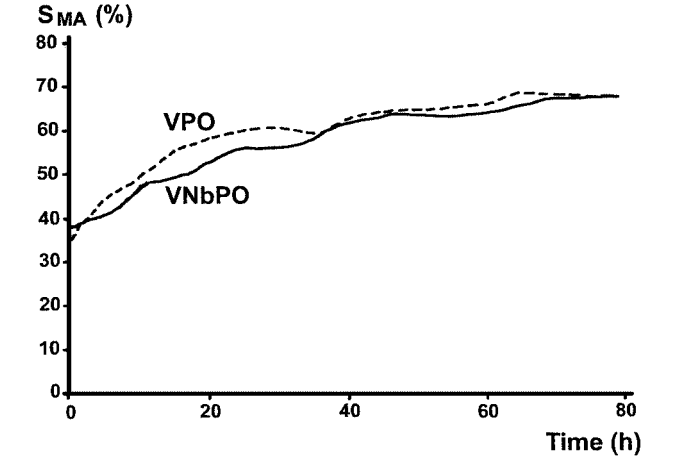

FIG. 5. Selectivity to maleic anhydride measured at 400°C under *n*-$C_4/O_2/He = 1.6/18.0/80.4$ at GHSV 2000 h^{-1} for the VNbPO and VPO catalysts as a function of time.

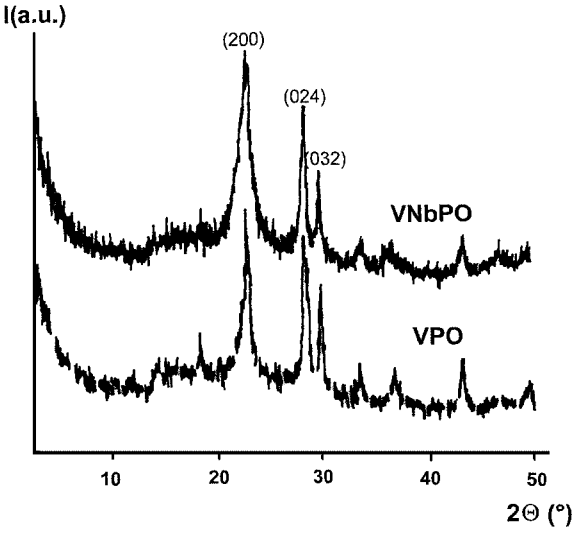

FIG. 6. XRD patterns of the activated VNbPO and VPO catalysts.

existence in V atoms in the unit $(VO)_2P_2O_7$ cell of four distinct oxidation states, at 4.44+, 4.19+, 3.79+, and 3.69+, respectively (22), in accordance with previous calculations of the individual bond strengths (23). We used these results to compare the oxidation states of V in the unit cell of $(VO)_2P_2O_7$ for the VNbPO sample with the undoped VPO catalyst from the spectra recorded at room temperature (Fig. 8). The two spectra are typical of a disorganized $(VO)_2P_2O_7$ catalyst with a complex signal around 2600 ppm. This complex signal, which is associated with the unit cell of $(VO)_2P_2O_7$, shows, for VNbPO, a global displacement to the right (contributions at 2740, 2176, and 1916 ppm), indicative of a higher oxidation state of V as compared to VPO. Signals at about 10 and 1140 ppm show

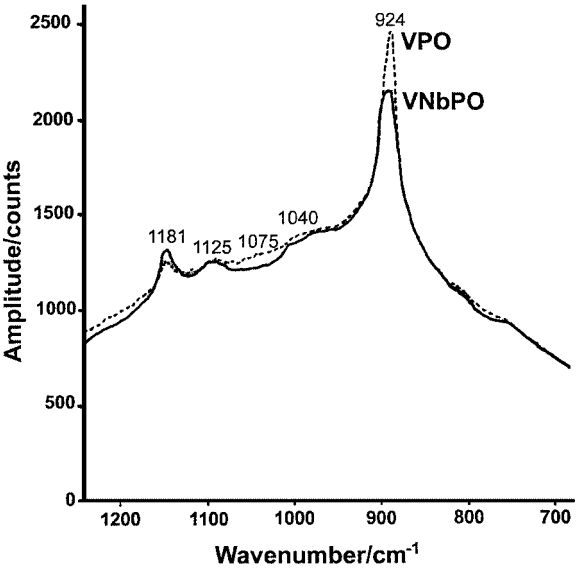

FIG. 7. Raman spectra of the activated VNbPO and VPO catalysts.

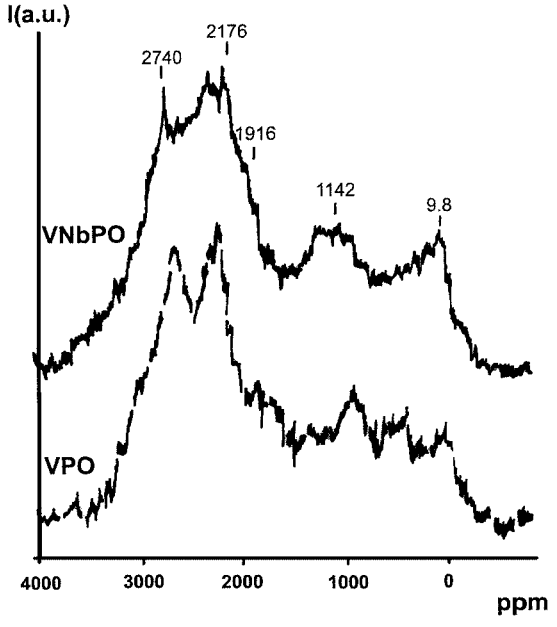

FIG. 8. ^{31}P NMR spectra by spin-echo mapping of the VNbPO and VPO activated catalysts.

the presence of V^{5+} entities attributed to either isolated V^{5+} species or V^{5+} microdomains and V^{4+}–V^{5+} dimers, respectively. The spectrum of VNbPO shows a higher contribution of signals associated with V^{5+} sites as compared to the spectrum of VPO. Finally, the comparison of the two ^{31}P NMR spectra by spin-echo mapping shows that VNbPO is globaly more oxidized than VPO.

XPS experiments have been performed on the activated catalysts to obtain information on the surface distribution of atoms. For the VNbPO catalyst, niobium was observed as Nb^{5+} with a binding energy of 208 eV. Previous studies have shown that the binding energies at the V $2p_{3/2}$ level for V^{4+} and V^{5+} are observed at 516.9 and 518.0 eV, respectively (24). The percentage of surface V^{4+} and V^{5+} of the two catalysts (as determined by XPS) has been calculated using a deconvolution method (25). Table 2 gathers together the XPS results obtained from the activated VPO and VNbPO catalysts. The relative distribution of surface O, V, C, and P atoms is similar for both catalysts, except for O, which is higher for VNbPO (66.9% as compared to 64.3% for VPO). The C concentration is lower for VNbPO (4.1%) as compared to VPO (7.3%), which may be indicative of less carbonaceous residues for the more oxidizing VNbPO catalyst. These observations favor a higher average oxidation state of the VNbPO catalyst as compared to the VPO one, as is experimentally observed by the higher percentage of surface V^{5+} (49%) in VNbPO, as compared to surface V^{5+} (29%) in VPO. The difference observed for the superficial C deposit may also be explained by the difference of morphology of the two catalysts. The P/V ratio is also slightly lower for VNbPO. It is important to notice a higher Nb/V surface ratio (Nb/V = 0.032) for the VNbPO catalyst as compared to the bulk composition (Nb/V = 0.010), indicating a Nb surface enrichment for this catalyst.

TABLE 2

Superficial Atomic Percentage and Atomic Ratios as Measured by XPS

	VPO (%)	VNbPO (%)
O 1s	64.3	66.9
V $2p_{3/2}$	10.9	11.2
	29 (V^{5+})–71 (V^{4+})	49 (V^{5+})–51 (V^{4+})
C 1s	7.3	4.1
Nb 3d	—	0.36
		Nb/V = 0.032
P 2p	17.5	17.4
	P/V = 1.60	P/V = 1.55

TEM examination showed that both catalysts have platelet morphologies and exhibit the characteristic surface-normal electron diffraction pattern of the [100] direction of $(VO)_2P_2O_7$ (Fig. 9). However the diffraction spots were less intense for VNbPO, which may be indicative of a lower crystallinity. The analysis of the images revealed a strong difference: while the periphery of the VPO crystals appeared quite regular in profile when viewed along the [100] direction, the periphery of the VNbPO crystals showed the existence of many kinks and steps in the same [100] direction. This was indicative of the existence of a high density of defects. EDX analysis of the platelet identified the presence of Nb in the whole crystal of the VNbPO catalyst.

Doping of $(VO)_2P_2O_7$ by Nb, i.e., the dissolution of Nb^{5+} into the lattice of vanadyl pyrophosphate, was evidenced, directly, by electrical conductivity measurements. Indeed, Fig. 10 shows the evolution of σ (in $\Omega^{-1} \cdot cm^{-1}$) with time under air for the two catalysts. The electrical conductivity σ of VNbPO is half an order of magnitude lower than that of VPO. $(VO)_2P_2O_7$ is known to be a *p*-type semiconductor (26), which suggests an *n*-doping character of Nb. The same observation was found when comparing the same materials calcined at 750°C under N_2. According to the valence induction law, described in Ref. (18), *n*-type doping by Nb may be explained by a substitution to V^{4+} by Nb^{5+} in $(VO)^{2+}$ according to the scheme

$$[(VO)_2P_2O_7] + [Nb^{5+}] \rightarrow V_{1-x}Nb_xO_2P_2O_{7+x}, \quad [4]$$

which is made possible because of the similar ionic radii of the corresponding cations: $Nb^{5+} = 6.4 \times 10^{-2}$ nm, $V^{4+} = 5.8 \times 10^{-2}$ nm.

For $(VO)_2P_2O_7$, a V^{4+} phase which is known to be a *p*-type semiconductor, the majority charge carriers are positive holes p^+ (i.e., electron vacancies), the existence of which is linked to the V^{5+}/V^{4+} redox couple

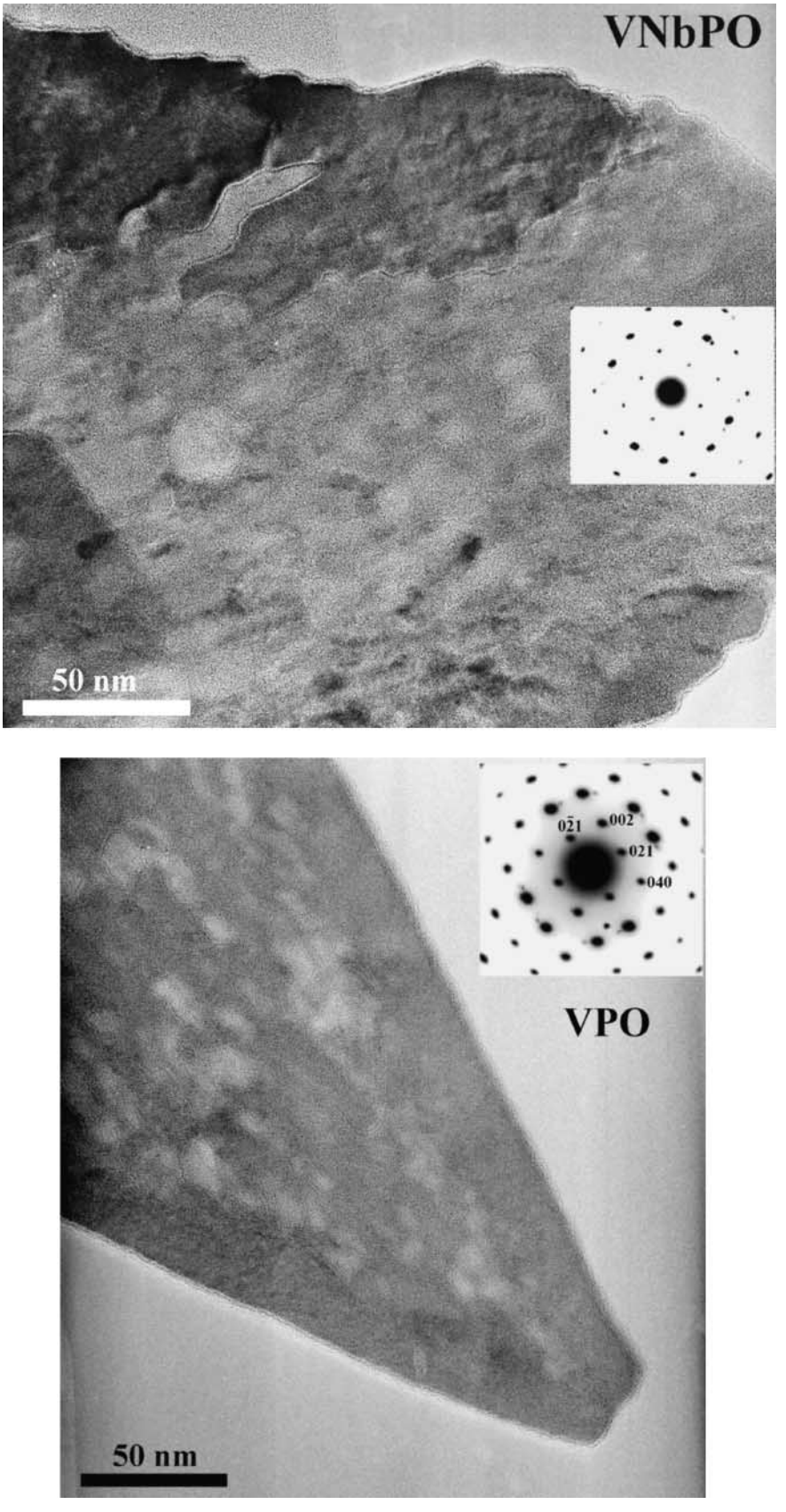

FIG. 9. TEM micrographs and electron diffraction patterns from the activated VNbPO and VPO catalysts.

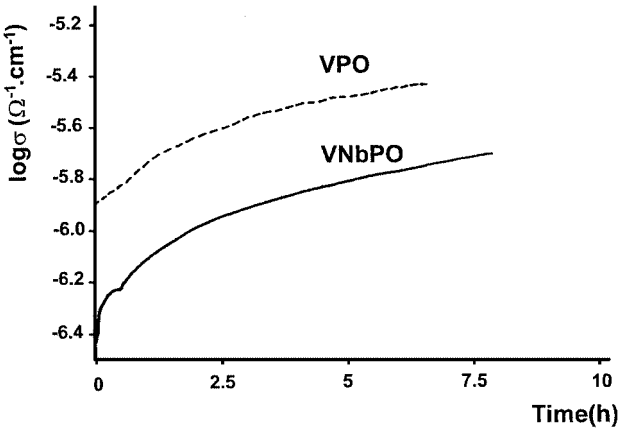

FIG. 10. Electrical conductivity measurements at 400°C under air for the activated VNbPO and VPO catalysts.

(associated with residual V^{5+} in $(VO)_2P_2O_7$) according to the equilibrium:

$$V^{5+} \leftrightarrow V^{4+} + p^+. \qquad [5]$$

The temporal increase of the electrical conductivity, observed for both catalysts, is indicative of gradual oxidation of the solids. Indeed, the p^+ entities are strong oxidizing agents, as observed in photocatalysis (27).

The initial activation step of the *n*-butane molecule, i.e., a C–H bond cleavage from a methylene group (28), involves a hole in the valence band of O^{2-} anions. At the surface (*S*), this hole can be filled by an electron hopping from a neighboring anion according to the scheme:

$$\left(O_S^{2-}\right)^0 + p^+ \leftrightarrow (O_S^-)^+. \qquad [6]$$

$(O_S^{2-})^0$ is a neutral entity with respect to the bulk solid, whereas $(O_S^-)^+$ is positively charged and constitutes the chemical support of the hole p^+. Therefore, O_S^- species are the oxidative ones for *n*-butane activation:

$$C_4H_{10} + (O_S^-)^+ \leftrightarrow C_4H_9^{\bullet} + H^+ + \left(O_S^{2-}\right)^0. \qquad [7]$$

The butyl radical $C_4H_9^{\bullet}$ subsequently reacts with a second O_S^- species to generate butene as the first reaction intermediate:

$$C_4H_9^{\bullet} + (O_S^-)^+ \leftrightarrow C_4H_8 + H^+ + \left(O_S^{2-}\right)^0. \qquad [8]$$

The two protons H^+ formed in Eqs. [7] and [8] are eliminated as water by reaction with one surface oxygen anion and by the formation of a doubly ionized anionic vacancy $(V_{O^{2-}})^{2+}$:

$$2H^+ + \left(O_S^{2-}\right)^0 \leftrightarrow H_2O + (V_{O^{2-}})^{2+}. \qquad [9]$$

The anionic vacancy $(V_{O^{2-}})^{2+}$ will be subsequently filled by dioxygen from the gas phase with the participation of one surface oxygen anion to regenerate the two holes $(O_S^-)^+$ involved in Eqs. [7] and [8]:

$$\left(O_S^{2-}\right)^0 + (V_{O^{2-}})^{2+} + \frac{1}{2}O_2 \leftrightarrow 2(O_S^-)^+. \qquad [10]$$

The overall redox process can be related to a Mars–van Krevelen mechanism. These results suggest that the initial step of *n*-butane activation on the V–P–O catalyst is the attack by O_S^- originating from the *p*-type semiconductor character of $(VO)_2P_2O_7$. The doping of the V–P–O catalyst by Nb^{5+} gives rise to a decrease of σ (Fig. 10) corresponding to a substitution to V^{4+} in $(VO)^{2+}$ by Nb^{5+} (Eq. [4]). The decrease in V^{4+} in $(VO)^{2+}$ sites implies the creation of additional or excess anionic oxygen $(O_S^{2-})^0$. (See Eq. [4].) This "constitutional" presence of excess anionic oxygen increases the concentration in oxidizing $(O_S^-)^+$ species, according to Eq. [6]. Since these species are responsible for the *n*-butane activation (Eqs. [8] and [9]), one observes a significantly higher conversion of *n*-butane as a function of the time of activation (Fig. 4).

By electron microscopy, the VNbPO catalyst showed a higher density of structural defects (Fig. 9). It may be inferred that it will be connected to an increase in the number of p^+ and of O^- species. The first step of the mechanism will be favored by an increase in the *n*-butane conversion, which is effectively observed. This result is confirmed by the increase in the V^{5+} surface density, as observed by XPS, since this goes in parallel with the density of p^+ entities (Eq. [5]).

For the VNbPO catalyst, however, the subsequent steps of the reaction mechanism will not be modified, as may be deduced from the similar selectivity profile when compared to VPO.

On $(VO)_2P_2O_7$, Lewis acidity has been explained by unsaturated cations or oxygen vacancies, associated with structural defects (29), while Brønsted acidity correlates with acid hydroxyl groups connected to P or V atoms (30, 31). By selective poisoning of acidic Brønsted sites, it was demonstrated that Brønsted acid sites (V–OH or P–OH) do not participate to the initial *n*-butane activation, since conversion was not inhibited in this case (32). Lewis acid sites associated with structural defects should be considered as the activating sites for *n*-C_4. Figure 11 shows the variation of the area of the characteristic pyridine bands (33) of Lewis sites at 1450 cm^{-1} and Brønsted sites at 1540 cm^{-1} as a function of the temperature of thermodesorption. It appears that there are globally fewer acid sites on VNbPO as compared to VPO. This figure provides interesting information on the influence of Nb doping on the relative distribution of these two types of acid sites: on both catalysts there are more Lewis sites as compared to Brønsted sites, which is generally observed on vanadium phosphorus oxide catalysts. However, there are many more Lewis sites of lower acidity (sites desorbing pyridine at a temperature lower than 250°C) on VNbPO as compared to VPO (sites desorbing pyridine at a temperature lower than 100°C). This result confirms the fact that Lewis acid sites

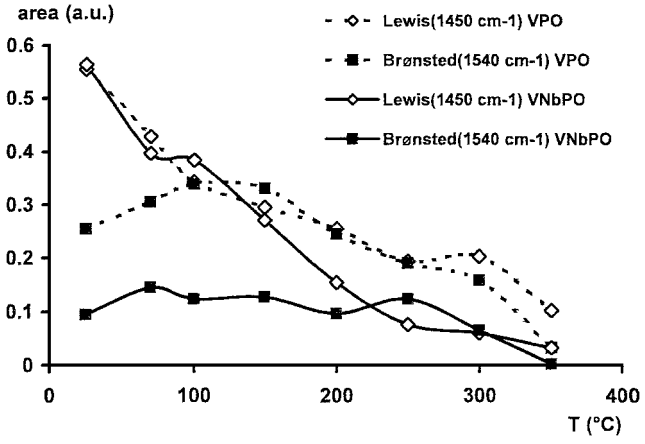

FIG. 11. Relative variation of the area of the Lewis (1450 cm^{-1} and Brønsted (1540 cm^{-1}) pyridine bands as a function of the temperature of desorption for VNbPO and VPO catalysts.

of lower acidity are associated with the structural defects. Indeed by Nb doping, as observed by electron microscopy, defect density is strongly increased and this enhances the number of weaker Lewis acid sites. We agree on the important role of Lewis acid sites, but, unlike previously published results (13), we disagree on the strength of their acidity.

Our studies (14; this publication) lead us to propose that Nb is located in close proximity to vanadium in the vanadium phosphorus oxide structure, near to a positive hole, which will facilitate the C–H bond breaking by surface O^- species. It should be noted that the V–O–Nb moiety has recently been proposed to be a paraffin activator (34).

CONCLUSIONS

This study has demonstrated that Nb may be used as an effective dopant to increase the conversion of *n*-butane for mild oxidation to maleic anhydride. The main interest of Nb stems from the increase in the number of defects at the periphery of $(VO)_2P_2O_7$ platelets, which increases the number of O-vacancies and facilitates the initial C–H activation of *n*-butane. These sites correspond to unsaturated cations which act as Lewis acid sites of low acidity. However, doping $(VO)_2P_2O_7$ by niobium does not improve the selectivity to maleic anhydride. It was observed that its presence changes the CO_2/CO product distribution in agreement with the higher V surface oxidation state of the VNbPO catalyst as observed by XPS.

ACKNOWLEDGMENTS

The authors are indebted to Vincent Martin for the SEM experiments, to Michèle Brun for the XPS measurements, and to Jean Billy for the acidity measurements. They thank CNPq (Conselho Nacional de Desenvolvimento e Pesquisa—Brazil) and CNRS (Centre National de la Recherche Scientifique—France) for the financial support of this work within the framework of a programme PICS (Programme International de Coopération Scientifique).

REFERENCES

1. Hodnett, B. K., *Catal. Rev.–Sci. Eng.* **27**, 373 (1985).
2. Centi, G., Trifiro, F., Ebner, J. R., and Franchetti, V. M., *Chem. Rev.* **88**, 55 (1988).
3. Hodnett, B. K., *Catal. Today* **1**, 477 (1987).
4. Hutchings, G. J., *Appl. Catal.* **72**, 1, 1991.
5. Zazhigalov, V. A., Haber, J., Stoch, J., Pyatnitzkaya, A. I., Komashko, G. A., and Belousov, V. M., *Appl. Catal. A* **96**, 135 (1993).
6. Ben Abdelouahab, F., Olier, R., Ziyad, M., and Volta, J. C., *J. Catal.* **157**, 687 (1995).
7. Sananès-Schulz, M. T., Ben Abdelouahab, F., Hutchings, G. J., and Volta, J. C., *J. Catal.* **163**, 346 (1996).
8. Sajip, S., Bartley, J. K., Burrows, A., Rhodes, C., Volta, J. C., Kiely, C. J., and Hutchings, G. J., *Phys. Chem. Chem. Phys.* **3**, 2143 (2001).
9. Mota, S., Volta, J. C., Vorbeck, G., and Dalmon, J. A., *J. Catal.* **193**, 319 (2000).
10. Hutchings, G. J., Desmartin-Chomel, A., Olier, R., and Volta, J. C., *Nature* **368**, 41 (1994).
11. Guliants, V. V., Holmes, S. A., Benzinger, J. B., Heaney, P., Yates, D., and Wachs, I. E., *J. Mol. Catal. A* **172**, 265 (2001).
12. Higgins, R., and Hutchings, G. J., U. S. Patent 4,418,003 (1983), assigned to Imperial Chemical Industries.
13. Matsuura, I., Ishimura, T., Hayakawa, S., and Kimura, N., *Catal. Today* **28**, 133 (1996).
14. de Oliveira, P., Eon, J. G., Chavant, M., Riché, A. S., Martin, V., Caldarelli, S., and Volta, J. C., *Catal. Today* **57**, 177 (2000).
15. Thorsteinson, E. M., Wilson, T. P., Young, F. G., and Kasai, P. H., *J. Catal.* **52**, 116 (1978).
16. Ciambelli, P., Lisi, L., Russo, G., Viparelli, P., and Volta, J. C., *Appl. Catal. A* **184**, 291 (1999).
17. Johnson, J. W., Johnston, D. C., Jacobson, A. J., and Brody, J. F., *J. Am. Chem. Soc.* **106**, 8123 (1984).
18. Herrmann, J. M., *in* "Catalyst Characterization, Physical Techniques for Solid Materials" (B. Imelik and J. C. Védrine, Eds.), p. 559. Plenum Press, New York, 1994.
19. Martin, V., Millet, J. M. M., and Volta, J. C., *J. Therm. Anal.* **53**, 111 (1998).
20. Ben Abdelouahab, F., Olier, R., Guilhaume, N., Lefebvre, F., and Volta, J. C., *J. Catal.* **134**, 151 (1992).
21. Sananès, M. T., Tuel, A., Hutchings, G. J., and Volta, J. C., *J. Catal.* **148**, 395 (1994).
22. Tuel, A., Canesson, L., and Volta, J. C., *Colloids Surf. A* **158**, 97 (1999).
23. Brown, I. D., and Wu, K. K., *Acta Crystallogr. Sect. B* **32**, 1957 (1976).
24. Garbassi, F., Bart, J. C., Tassinari, R., Vlaic, G., and Lagarde, P., *J. Catal.* **98**, 317 (1986).
25. Abon, M., Bere, K. E., Tuel, A., and Delichere, P., *J. Catal.* **156**, 25 (1995).
26. Herrmann, J. M., Vernoux, P., Bere, K. E., and Abon, M., *J. Catal.* **160**, 106 (1997).
27. Herrmann, J. M., *Catal. Today* **53**, 115 (1999).
28. Pepera, M. A., Callahan, J. L., Desmond, M. J., Milburger, E. C., Blum, P. R., and Bremer, N. J., *J. Am. Chem. Soc.* **107**, 4883 (1985).
29. Busca, G., Centi, G., and Trifiro, F., *Appl. Catal.* **25**, 265 (1986).
30. Centi, G., Trifiro, G., Busca, G., Ebner, J. R., and Gleaves, J., *Faraday Discuss. Chem. Soc.* **87**, 215 (1989).
31. Cornaglia, L. M., Lombardo, E. A., Anderson, J. A., and Garcia Fierro, J. L., *Appl. Catal. A* **100**, 37 (1993).
32. Centi, G., Colinelli, G., and Trifiro, F., *Appl. Catal.* **48**, 13 (1989).
33. Knözinger, H., *Adv. Catal.* **184**, 25 (1976).
34. Grasselli, R. K., *Top. Catal.* **15**(2–4), 93 (2001).